LAWRENCE
LIVERMORE
NATIONAL
LABORATORY

LLNL-TR-783346

CMDV-RRM: Representation of Clouds and Convection across scales in E3SM

J. C. Golaz, S. Xie, X. Zheng, W. Lin, T. Zhang, S. Endo, A. Vogelmann, R. Jackson, S. Collis, E. L. Roesler, B. Hillman, P. Bosler, M. McChesney, M. Zhang

July 26, 2019

Disclaimer

This work performed under the auspices of the U.S. Department of Energy by Lawrence Livermore National Laboratory under Contract DE-AC52-07NA27344.

Final Report

CMDV-RRM: Representation of Clouds and Convection across scales in E3SM

July 31, 2019

LLNL
Chris Golaz (PI), Shaocheng Xie (co-PI), Xue Zheng

BNL
Wuyin Lin, Tao Zhang, Satoshi Endo, Andrew Vogelmann

ANL
Robert Jackson, Scott Collis

SNL
Erika L. Roesler, Ben Hillman, Pete Bosler, Matt McChesney

Stony Brook University
Minghua Zhang

LLNL-TR-783346

Lawrence Livermore National Laboratory is operated by Lawrence Livermore National Security, LLC, for the U.S. Department of Energy, National Nuclear Security Administration under Contract DE-AC52-07NA27344.

1 Overview

In order to address mission-relevant questions, DOE's Energy Exascale Earth System Model (E3SM) is pushing the limits of horizontal resolution among global Earth System Models (ESMs). The atmospheric resolution in the recently released E3SMv1 is 110 km in the standard configuration, and 25 km in the high-resolution configuration (Golaz et al., 2019).

Furthermore, E3SM is fairly unique among global ESMs with a capability for multiresolution modeling using refined grids in most of its components (atmosphere, land, ocean, sea-ice). This Regionally Refined Model (RRM) capability is critical for future E3SM simulation campaigns that have a strong regional focus to meet DOE's needs in support of energy-sector decisions. RRM grids are also particularly well suited for model evaluation and process-level studies taking advantage of the vast amount of ASR site data collected over the past several decades.

The overarching goal of this project was to understand and improve the behavior of clouds and convection in E3SM across these scales using RRM. Key deliverables that resulted from the project are summarized below, with more details provided in the subsequent sections of the report.

- **E3SM RRM grids** focused on ARM sites: SGP, TWP and ENA as well as new grids designed for upcoming E3SMv2 simulations campaigns ("North America" for the Water Cycle campaign and "Antarctica" for the Cryosphere campaign).
- **Datasets**
    - High-resolution 3D variational analysis of atmospheric states at 2km x 2km resolution from dynamically constrained WRF GSI and WRF simulations for the ARM MC3E May 20, 2011 convective event.
    - 17 years of quality controlled corrected radar volumes, echo top heights, and rainfall rates from the CPOL Radar in Darwin.
    - 8 years of 3D winds derived from the CPOL Radar and ERA Interim over Darwin.
    - E3SMv1 hindcast (CAPT) and free running simulations with CONUS RRM and 1 deg uniform grids.
    - E3SMv1 hindcast (CAPT) simulations with ENA RRM and 1 deg uniform grids during the ARM CAP-MBL field campaign (June 2009 to December 2010).
- Analyses of **E3SMv1 simulations** over CONUS, TWP and ENA. The analyses of CONUS and TWP uncovered issues with the representation of deep convection by the Zhang-McFarlane convection parameterization in E3SMv1.
- **E3SM model developments** aimed at addressing these issues:
    - Improved parameterized deep convection. A new trigger based on dynamic convective available potential energy (dCAPE) and removal of the restriction that convection must be rooted at the surface (Unrestricted Launch Level; ULL). These modifications result in improved precipitation intensity, diurnal cycle as well as

help capture elevated convection. We anticipate that these developments will be incorporated in E3SMv2.
    - In addition, a convective trigger function based on machine learning is also being developed. This novel trigger function uses the classification model XGBoost, a highly efficient and scalable tree-based gradient boosting model. It is trained and tested using long-term constrained variational analysis forcing data from ARM SGP and GoAmazon. Results to date indicate that the XGBoost ensemble classification algorithm substantially outperforms conventional convective trigger functions.
- **Tools**
    - **PyDDA** (Pythonic Direct Data Assimilation): A Pythonic Multiple Doppler Radar Wind Retrieval Package developed as part of the processing of CPOL data. PyDDA is available publicly and will be used by NASA for ground validation of GPM vertical velocities in their Decadal Plan.
    - **TINT** (TINT Is Not TITAN): A long-term cell tracking package that works directly with the Py-ART grid object in Python and is based on the Thunderstorm Identification, Tracking, Analysis and Nowcasting package (TITAN).
    - **StrideSearch**: a tool originally designed for identifying and tracking tropical and extratropical cyclones in global model output. This project supported further development of StrideSearch to search on unstructured grid meshes (such as E3SM RRM grids) instead of exclusively latitudinal-longitudinal cartesian grids, search with a kd-tree algorithm, and search for mesoscale convective systems.
    - **Multi-Objective Optimization Framework**: a new parameter calibration and optimization package for multi-resolution E3SM model tuning. The package can optimize regional objectives for both low- and high-resolution (or RRM) configurations with global metrics from the low-resolution as constraints.
- **15 peer-reviewed publications.**

2 Regionally Refined Model (RRM) Configurations

The atmospheric resolution of E3SMv1 in its standard configuration is 1 degree (~110 km). This increases to ¼ degree (~25 km) in the high-resolution configuration of E3SMv1. While global coupled high-resolution simulations are possible with E3SMv1 on DOE supercomputing resources, simulations campaigns are limited to a total of 100 to 200 years. On the other hand, simulation campaigns with the standard resolution of E3SMv1 can be much more extensive (2000 years or more) and cover a wider range of forcing scenarios and ensemble size, but without providing the high-resolution details.

RRM configurations can bridge the gap between these two use-cases: they offer the benefit of higher resolution over regions of interest, but at a much-reduced computational cost (typically 6 to 8x cheaper), thus allowing for more extensive simulation campaigns. While E3SMv1 focused mostly on globally uniform grids, the upcoming E3SMv2 will rely on RRM for a majority of its simulation campaign.

Qi et al. (2019) compared EAMv1 RRM with a 25 km refined patch over the contiguous United States (CONUS) to its corresponding globally uniform 110 and 25 km configurations, as well as to observations and reanalysis data. Their results indicated that RRM can serve as a useful tool to test physical schemes across different scales for improving scale awareness of the physics in future E3SM versions. It also provided additional confirmatory evidence that the RRM is an efficient and effective approach for high-resolution model development and hydrologic research.

As part of this project, SNL developed new RRM configurations as well as maintained existing ones for E3SM. We focused on five configurations. All five grid configurations had a low-resolution of 1-degree (~110km) and a high-resolution static patch of 1/4-degree (~25km). The high-resolution patches focused on Atmospheric Radiation Measurement (ARM) sites to further improve model development by housing a “ground-truth” based on ARM measurements and value-added products. These RRM meshes and their corresponding sites (in parentheses) include CONUS (SGP), North America (SGP and Barrow-NSA), ENA (ENA), TWP (TWP), and a mobile facility for the intensive operation period ARM West Antarctic Radiation Experiment (AWARE). Figure 1 shows the relative locations of the ARM sites. This project initially proposed looking at the hydrostatic limit within the RRM configurations, but resources did not allow for this development in the three-year time period.

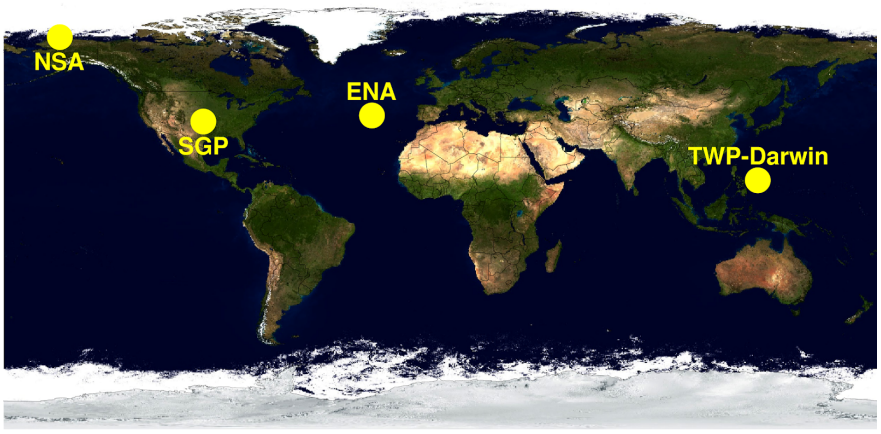

Figure 1. The map of the relative locations of the ARM sites.

Decisions on the size and shape of the grids were developed within the team as well as discussed with the greater E3SM community. For example, for the ENA and TWP grids, Figure 2 shows some of the proposed grid designs for ENA (left), and the constraints of the TWP grid defined by precipitation retrievals (right).

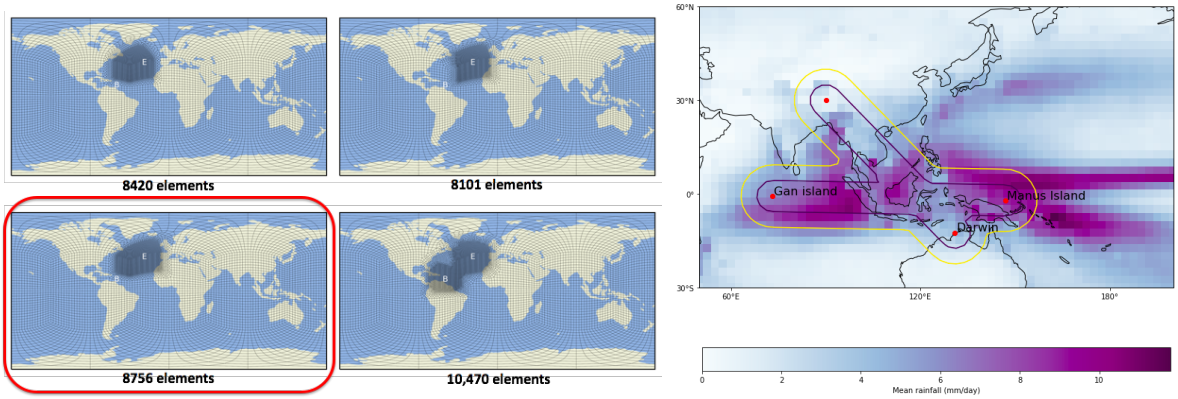

Figure 2. (Left) some of the proposed grid designs for ENA, and (right) the constraints of the TWP grid defined by precipitation retrievals.

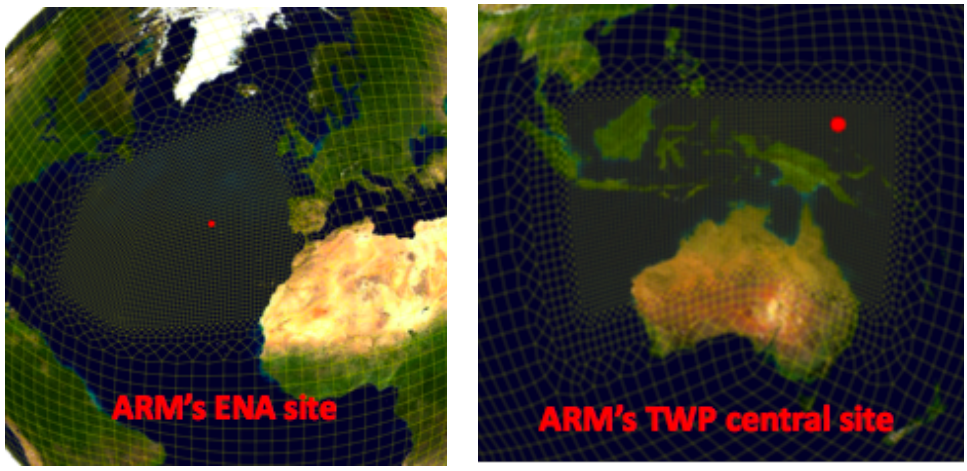

Figure 3. **(Left)** the final geometry of the ENA grid, and **(right)** the TWP grid.

The final geometry of the ENA and TWP grids are shown in Figure 3. The ENA and TWP RRM grids were added to the E3SM Github repository in August 2017. Since E3SM is an open source, open development project, the new grids are available to anyone interested.

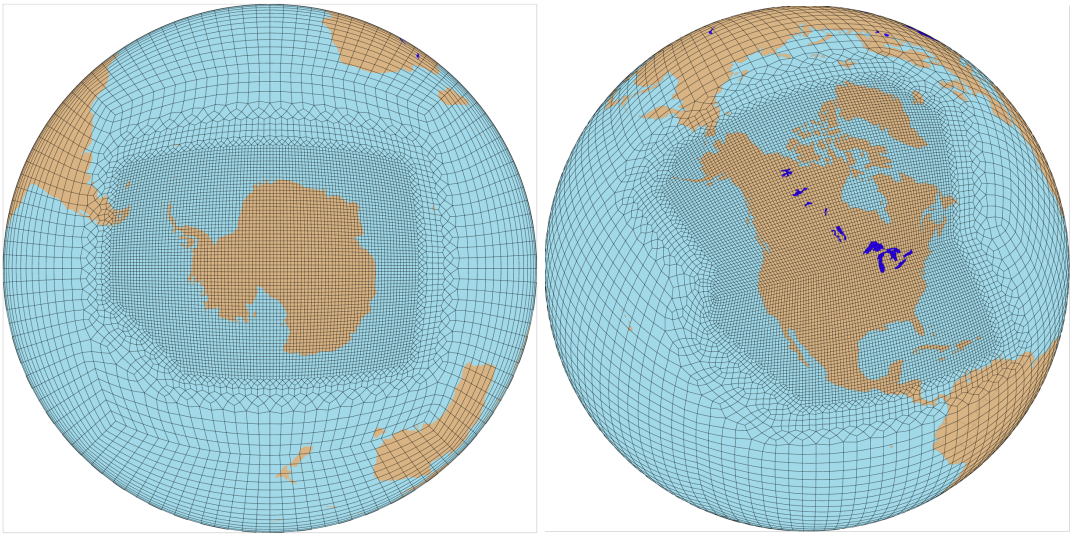

Figure 4. **(Left)** Antarctica Grid for E3SM v2 Cryosphere Experiment containing 12,209 elements. **(Right)** North America Grid for E3SM v2 Water Cycle Experiment containing 14,454 elements.

Portions of this project were merged with E3SMv2 development efforts at the end of CY 2018. Upon this redirection, two additional RRM grid configurations were requested for the Cryosphere and Water Cycle simulation campaigns. The Antarctica grid (Figure 4 left), and the North America grid (Figure 4 right) were added to the E3SM repository in July, 2019. Simulations using these grids are to be performed by E3SMv2 Core Development team members in CY 2019 and CY 2020.

During the course of this project, it became clear that the process of generating new RRM grids and all the supporting input datasets is long and tedious, with many steps often poorly documented. Due to the heightened interest in regional grid refinement, E3SM decided to invest resources to simplify and streamline that process. Ben Hillman who was originally trained in the "art" of atmosphere grid generation as part of this project is now leading an effort to develop a streamlined grid generation procedure as part of an E3SM NGD (Next Generation Development) effort. We expect that the streamlined procedure will significantly speed up the creation of future RRM grids.

3 Datasets

To facilitate model evaluation, this project constructed a number of new datasets based on ASR observations. These datasets were analyzed internally, but have also been released publicly. SBU developed a new 3D-ARM-VAR analysis product for the SGP site. ANL collaborated with the Bureau of Meteorology to process 17 years of data from the TWP C-band Polarization Radar (CPOL) in order to develop a climatology of echo top height, rainfall rate, and three-dimensional winds.

3.1 3D-ARM-VAR analysis

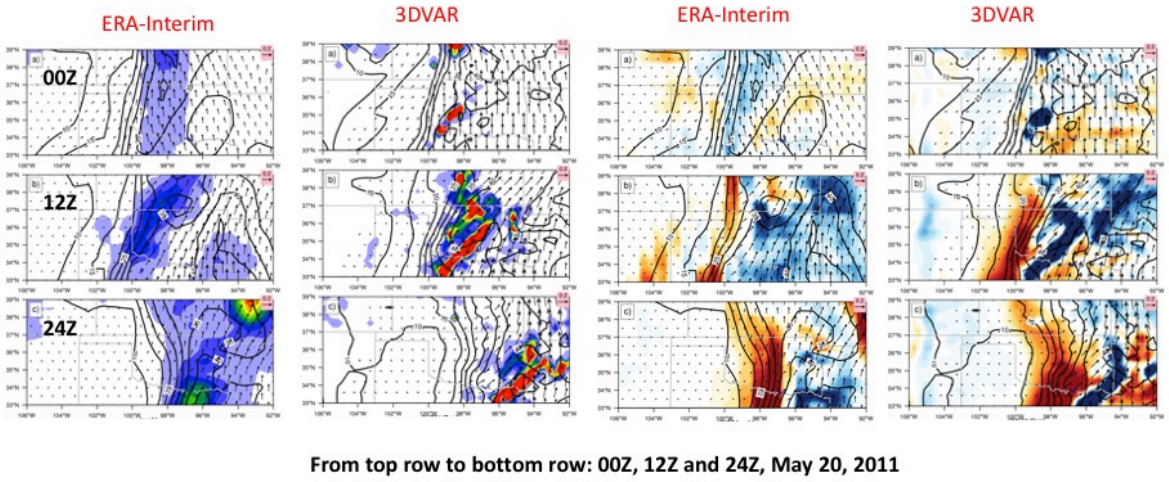

Figure 5. Two left columns: ERA-Interim and 3D-ARM-VAR analysis over the SGP of the vertically-integrated moisture flux (vector), 850hPa geopotential height (contour), and precipitation (shading). Two right columns: same as the two left columns except that the color shading represents the vertically integrated moisture convergence. Panels from top to bottom are for 00 UTC, 12 UTC, and 24UTC on May 20, 2011 during the ARM MC3E IOP.

For the 3D-ARM-VAR analysis, SBU derived three-dimensional atmospheric fields that are consistent with high-resolution measurements of surface precipitation by integrating a suite surface and atmospheric measurements during ARM MC3E (Figure 5). The two left columns show, from top to bottom for 00 UTC, 12 UTC, and 24UTC on May 20, 2011, the vertically-integrated moisture flux (vector), 850hPa geopotential height (contour), and precipitation in ERA-Interim (shading) and in the 3D-ARM-VAR product. The precipitation in the 3D-ARM-VAR product is the same as from the radar observation. It can be seen that while ERA-Interim captures the precipitation event, the intensity at the convective scale is severely underestimated. The two right columns in the figure are the same as those in the left two columns except that the color shading represents the vertically integrated moisture convergence. In 3D-ARM-VAR, the total moisture convergence closely mirrors the observed precipitation. This is not the case in the ERA-Interim.

The 3D-ARM-VAR product is therefore better suited as forcing data to single-column and cloud resolving models, as well as E3SM model evaluation compared to ERA-Interim. The data is publicly available[1].

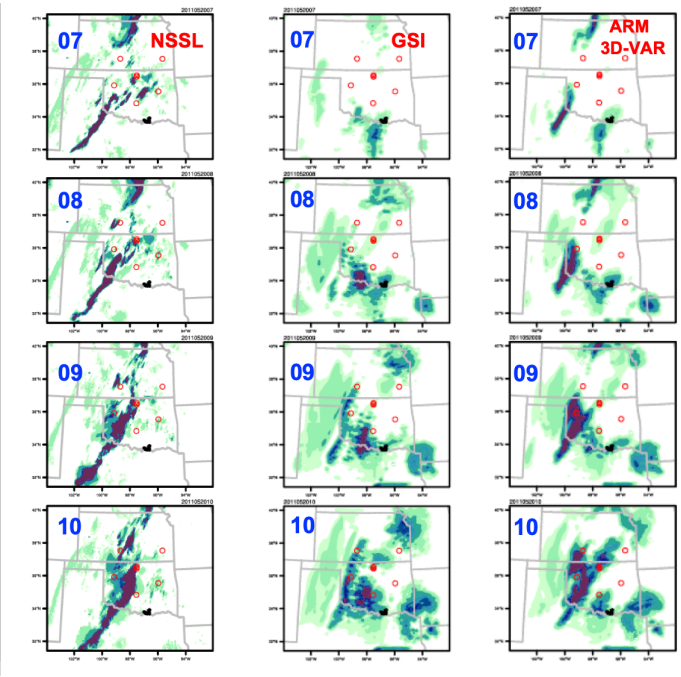

Figure 6. (Left) hourly precipitation from 07 UTC to 10 UTC from the NSSL radar product. (Middle) WRF forecast with initialization at 06 UTC using initial condition from the standard GSI assimilation system. (Right) WRF forecast with initialization at 06 UTC using 3D-ARM-VAR as initial condition.

The 3D-ARM-VAR product has also been evaluated as initial condition for WRF. The first column of Figure 6 shows the hourly precipitation from 07 UTC to 10 UTC on May 20, 2011 over the SGP from the NSSL radar product. The middle column shows a WRF forecast of hourly precipitation when it is initialized at 06 UTC by using assimilation from the operational GSI as initial condition. The right column shows the WRF forecast of hourly precipitation when it is initialized at 06 UTC by using 3D-ARM-VAR as initial condition. As can be seen, 3D-ARM-VAR as initial condition dramatically improves the hour-one forecast of the initial precipitation band and its subsequent evolution.

[1] http://cloud.somas.stonybrook.edu/mzhang/arm/MC3E/

3.2 CPOL derived datasets

One goal of CMDV-RRM was to test the performance of the convective parameterization in resolving convection over the TWP site in Darwin. To do so, a climatology of relevant variables needed to be created from decadal observations. ANL used 17 years of data from the C-band Polarization Radar (CPOL) in order to develop a climatology of echo top height, rainfall rate, and three-dimensional winds. We assisted the Bureau of Meteorology in creating a processing package for the CPOL data using Py-ART (Helmus and Collis 2016). This processing package included a careful calibration of the data using relative calibration adjustment (Louf et al. 2018). In addition, given that both the monsoon and the MJO are important factors that can heavily influence the strength and structure of convection over Darwin, we have tagged this dataset by the corresponding phase of the monsoon and MJO. We plan on releasing all of these products to the ARM archive for use by the community during August.

3.2.1 Radar estimated storm top heights

Various techniques were considered in order to develop the climatology of echo top heights. Radar reflectivity thresholds are typically used to define cloud boundaries, but these can be prone to attenuation and issues with radar sensitivity when examining clouds far away from the radar. Therefore, we instead used a technique that relies on velocity texture, a measure of the spatial variability in Doppler velocities. Higher velocity textures correspond to clear air and artifacts, while lower values typically correspond to hydrometeors. In the end, we found it optimal to use the lowest gate in the column where velocity texture is greater than 3 to define the echo top height.

These cloud top heights were then segregated into different phases of the MJO and monsoon. It was found that the distribution of these cloud top heights was sometimes bimodal, with one mode corresponding to cumulus congestus with tops of around 2 to 4 km and the other mode at 7 to 9 km. This bimodality was more commonly observed when the active phase of the MJO was over Australia. In addition, we observed that, during the day, the convection was more typically present over the Tiwi Islands and the coast of Australia, while at night it was typically present over the oceans as shown in Figures 7-8. There is also a well-defined peak of occurrences over the Tiwi Islands that corresponds to Hector, an intense storm that occurs nearly daily over the Tiwi Islands that is formed from sea-breeze convergence over the mountains of the Tiwi Islands. These results were published in Atmospheric Chemistry and Physics (Jackson et al. 2018).

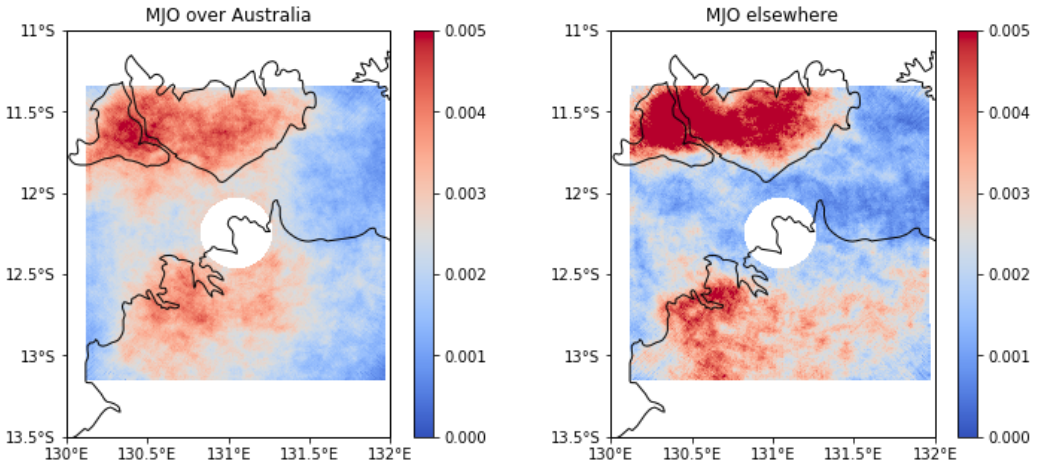

Figure 7. Normalized frequency of occurrence of ETHs > 7 km during the day when the active phase of the MJO is **(left)** over Australia and **(right)** away from Australia.

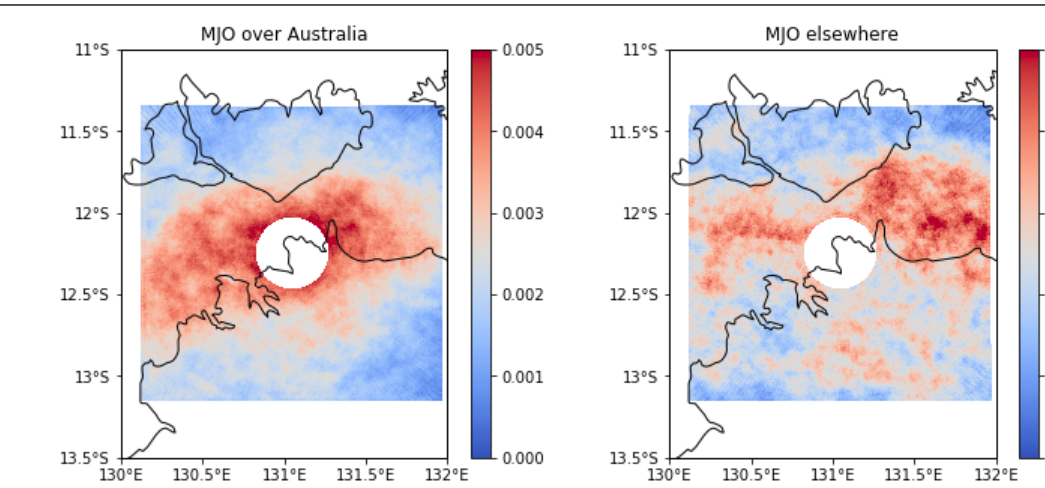

Figure 8. As Figure 7, but at night.

3.2.2 Winds

In order to derive the 3D wind fields from the CPOL data, we needed to develop a scalable multiple Doppler retrieval package that can be applied to the data. While Multidop was available for use as a wind retrieval package that was able to ingest Cf-Radial CPOL data, this package is not scalable to datasets as large as CPOL's. This therefore motivated us to develop PyDDA, a new multiple Doppler retrieval package written entirely in Python. PyDDA is publicly available[2], allowing anyone in the scientific community to use it.

[2] https://openradarscience.org/PyDDA

The estimation of vertical winds from networks of radars can be highly uncertain due to many factors that include assumptions made by the retrieval regarding the mass continuity equation, fall speeds of particles, as well as decreased sampling by the radars aloft. This therefore warranted an investigation of the uncertainty of vertical velocity retrievals from the CPOL and Berrimah radars in Darwin. This was done using the Cloud Resolving Model Simulator (CRSIM) that takes in cloud resolving model data with given radar configurations and produces simulated radar fields from such configurations. In collaboration with BNL, we therefore used CRSIM to create simulated Doppler velocity and reflectivity fields from a WRF run of the 20 Jan 2006 TWP-ICE monsoonal convection event and then retrieved 3D winds from the simulated radar data given a configuration of 2 radars and 15 or 60 elevation scans. The original configuration of CPOL and Berrimah used 15 elevation scans, so the left panel of Figure 9 is most representative of the available radar configuration and shows greater than 5 m/s differences between the winds from the retrievals and the original WRF winds. Figure 9 shows that increasing the number of elevation scans drastically improves the agreement between the retrieval and the original model vertical velocities. In addition, we found that using 3 or more radars also improves the agreement substantially. Therefore, this shows that there is likely inadequate sampling by the radars for the use of reliable vertical velocity retrievals. In the final data product, we will produce a version with 3D winds from Berrimah and CPOL as well as 2D winds from CPOL and ERA-Interim.

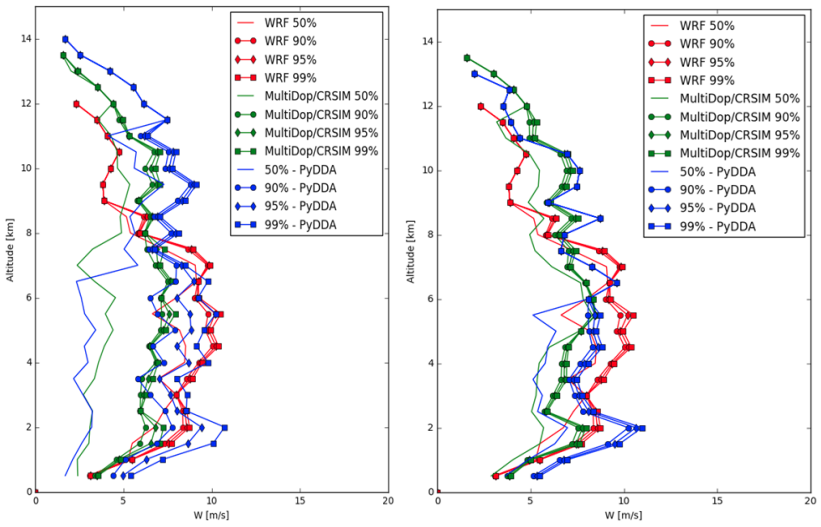

Figure 9. Probability Density Functions (p.d.f.s) of vertical velocities retrieved from the simulated radar data from the WRF simulation of the 20 Jan 2006 TWP-ICE convective event. Red lines denote the WRF vertical velocities, while the blue lines denote those retrieved by PyDDA from the simulated data and the green line denote vertical velocities retrieved by the Multidop package for comparison. **(Left)** p.d.f.s using 15 elevation scans from a 2-radar configuration, **(right)** p.d.f.s using 60 elevation scans from a 2-radar configuration.

3.2.3 Rainfall rates

We estimated the rainfall rates from the CPOL radar moments. In order to do this, power law fits of rainfall rates as a function of simulated moments from the Video Disdrometer data were produced using PyDSD. In addition, statistical uncertainties in these fits were estimated by subtracting the quartiles of rain rate over given ranges of radar moments. These power law fits were then used to estimate rainfall rates from the CPOL dataset. The rainfall rates from the gate immediately above the disdrometer were then compared against the video disdrometer observations. In the end, we found that rainfall rates produced by the "CSU-blended" technique (Thompson et al. 2018) were in the best agreement with the VDIS observations.

These rainfall rates were then separated into differing phases of the MJO and monsoon in order to characterize the diurnal cycle of rainfall over Darwin that can be used as an observational target for E3SM. For example, Figure 10 shows the peak hour of maximum rainfall from the CPOL dataset. There is a very strong signature in the peak hour of rainfall during break conditions with rainfall rates peaking near sunrise over the oceans and over the afternoon in the land. The peak in the afternoon is likely due to convection forced by diurnal heating which would be more common in break conditions where there is less cloud cover. The morning peak of rainfall over the ocean may be attributable to mesoscale convective systems that form overnight over the ocean as a result of differential radiative cooling between the clear and cloudy areas that induces surface convergence (i.e. Gray and Jacobson 1975).

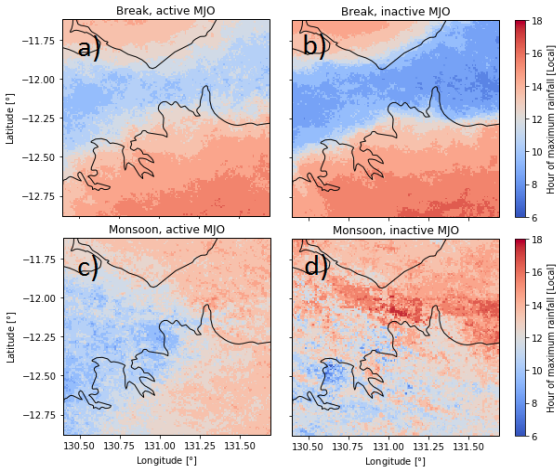

Figure 10. The average peak hour of rainfall for the 17-year study period in **(a)** active MJO/break conditions, **(b)** suppressed MJO/break conditions, **(c)** active MJO/monsoon conditions and **(d)** inactive MJO/monsoon conditions.

4 Analysis and model evaluation

4.1 Analysis of CMIP5 models

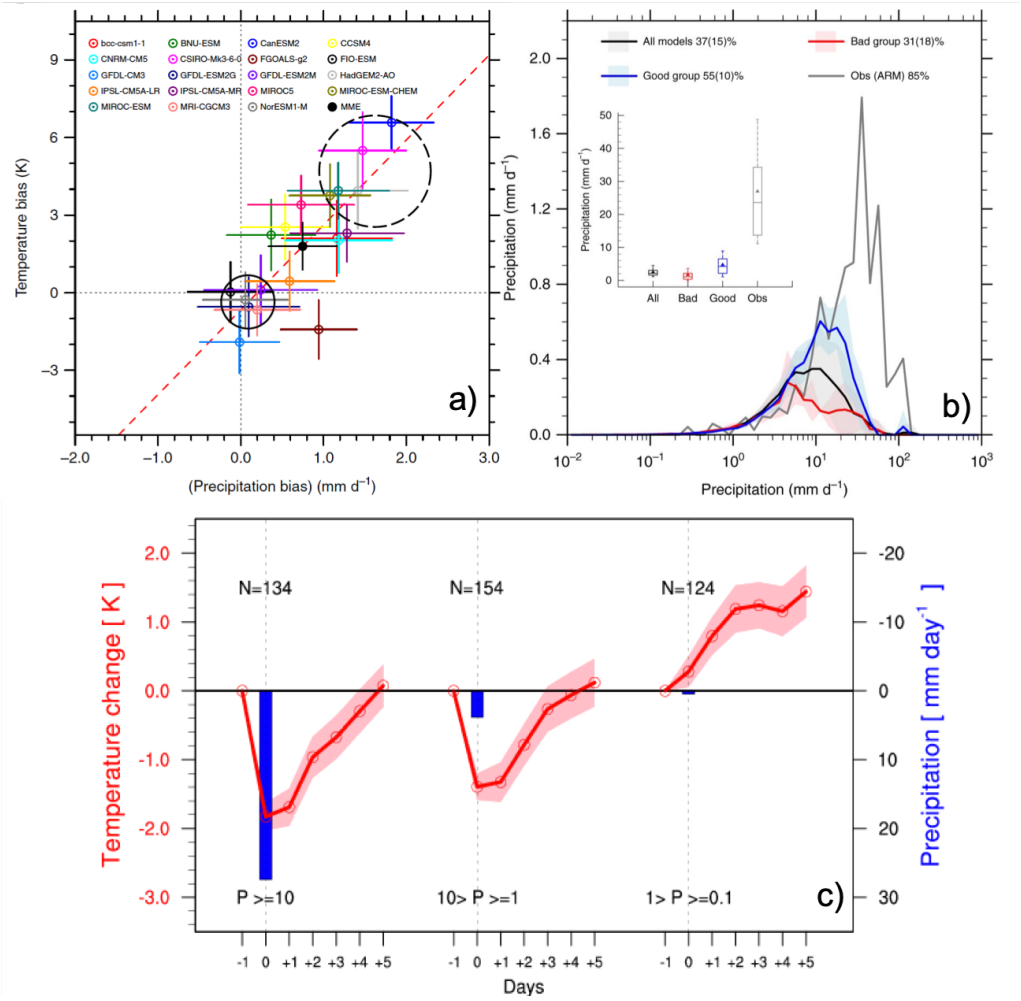

Figure 11. (a) Scatter plot of the summertime temperature bias and precipitation bias over the central U.S. among CMIP5 historical model simulations during the reference period 1979-2005. Colors represent different models. Solid dot indicates the ensemble mean while horizontal and vertical colored lines indicate one standard deviation. The red dash line indicates the least-square linear fit among the models. The solid (dash) circle contains the models selected as "good" ("bad") group based on precipitation intensity distribution in **(b)**. **(c)** Relative change of surface temperature (left *y*-axis) within a week after three different intensity categories of rainfall events (right *y*-axis). Numbers *N* indicate the sample sizes in each rainfall categories.

SBU collaborated on a project analyzing CMIP5 models using long-term ARM measurements at the SGP to investigate the cause of summer-time warm and dry biases common to most climate models (Figure 11a). E3SM suffers from similar biases (see Section 4.2 below). We found that most of the models underestimate the precipitation intensity over the SGP (Figure 11b) because they cannot simulate mesoscale convective systems. Models that severely underestimate precipitation (red line in Figure 11b) also have the largest warm biases in temperature. The observed precipitation events are shown to be followed by a period of surface cooling for several days, with larger precipitation followed by stronger cooling (Figure 11c). Using ARM data, we were able to show that the surface cooling following the precipitation events can be attributed to increased amount of shallow convective clouds, which lead to less solar radiation at the surface, and thus cooling. Results from this work have been published in Lin et al. (2017, Nature Communication).

4.2 Validating E3SMv1 with CAPT simulations with CONUS RRM

LLNL conducted short-term hindcast simulations with E3SMv1 for the summer of 2011 using the Cloud-Associated Parameterizations Testbed (CAPT) protocol, in which large-scale atmospheric state variables are constrained with reanalysis data. We conducted three CAPT experiments for the summer of 2011 (Table 1): 1) the ne30 (1 degree) uniform resolution and the EAMv1 (E3SMv1 Atmosphere Model) with ne30 parameterization setting (i.e. ne30_NE30TP_CAPT); 2) the CONUS RRM grid and the EAMv1 ne30 parameterization setting (i.e. RRM_NE30TP_CAPT); and 3) the CONUS RRM grid and the EAMv1 ne120 (1/4 degree) parameterization setting (i.e. RRM_NE30TP_CAPT).

Table 1. The summary of the EAMv1 simulations

Experiments*	**Simulation type**	**Model grid**	**Tuning parameters**
ne30_NE30TP_CAPT	CAPT Day2	ne30	NE30
RRM_NE30TP_CAPT	CAPT Day2	CONUS RRM	NE30
RRM_NE120TP_CAPT	CAPT Day2	CONUS RRM	NE120
ne30_NE30TP_AMIP	AMIP	ne30 (1°)	NE30
RRM_NE30TP_AMIP	AMIP	CONUS RRM (1 to 0.25°)	NE30
RRM_NE120TP_AMIP	AMIP	CONUS RRM	NE120

* The name of each experiment is defined by the model grid, the tuning parameters from ne30 or ne120, and the experiment type (CAPT or AMIP).

For each CAPT experiment, a series of three-day global hindcasts are initialized at 0000 UTC every day with the European Centre for Medium-Range Weather Forecasts (ECMWF) ERA-Interim reanalysis data for the period between 31 May and 31 August in 2011. Therefore, we have

a total of 93 three-day hindcasts for each CAPT experiment. Allowing for a 1-day model spin-up period, we concatenate the model output from the second day of each hindcast to get a CAPT Day2 dataset for the time period from 1 June, 2011 to 31 August, 2011. Atmospheric initial conditions related to aerosol and clouds are generated from a longer-term EAMv1 simulation from October 2010 to August 2011 with the same setting as the CAPT experiment, in which the horizontal velocities are nudged toward ERA-Interim reanalysis data. To minimize the differences in the land initial conditions between the simulations at different model resolutions, the land initial condition for ne30_NE30TP_CAPT is re-gridded from the land initial condition for RRM_NE30TP_CAPT.

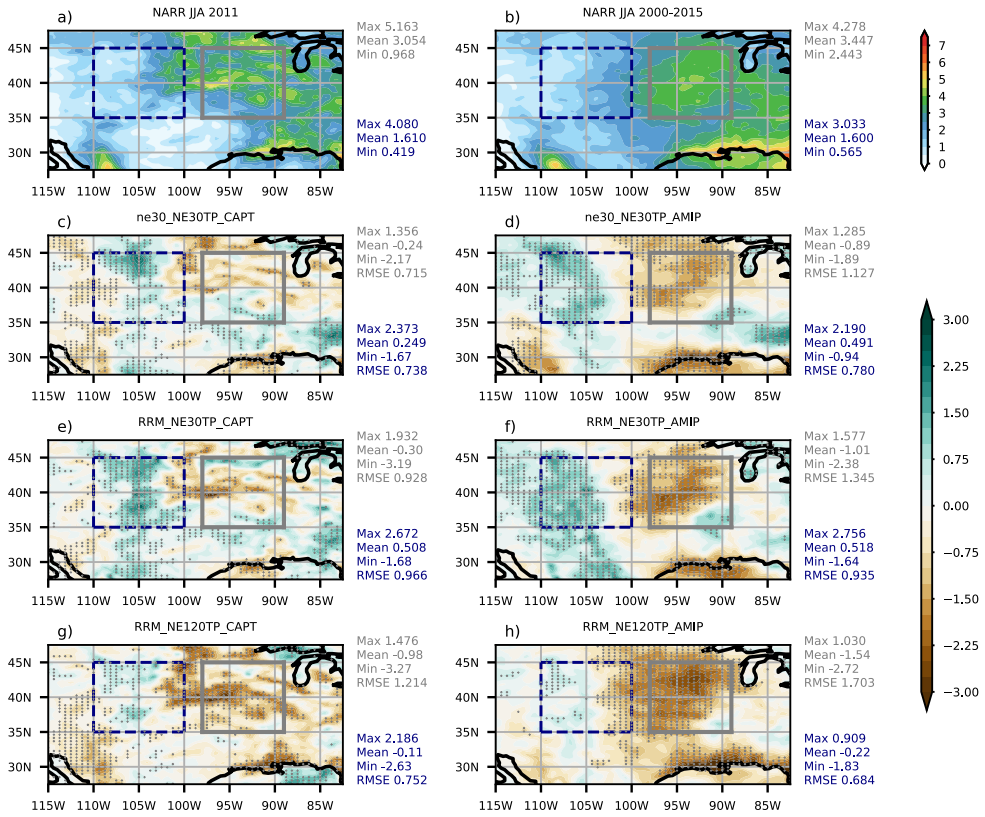

Figure 12. JJA seasonal mean precipitation (unit: mm/day) from NARR reanalysis over the time period **(a)** 2011, and **(b)** 2000-2015. The difference between **(c)** NE30_NE30TP_CAPT, **(e)** RRM_NE30TP_CAPT, **(g)** RRM_NE120TP_CAPT and the NARR reanalysis for the year 2011; and the difference between **(d)** ne30_NE30TP_AMIP, **(f)** RRM_NE30TP_AMIP, **(h)** RRM_NE120TP_AMIP and the NARR reanalysis (2000-2015) data. Naming convention is described in Table 1. The navy dash rectangle indicates the study area of the Rocky Mountain (35°N-45°N, 110°W-100°W). The gray rectangle (35°N-45°N, 98°W-89°W) indicates the Great Plains. The domain mean statistics for the Rocky Mountain region and the domain mean statistics for the Great Plains are listed in the navy text and the gray text, respectively. Stippled regions indicate where the difference reaches the 95% confidence level based on a 2-tailed Student's t-test.

In addition to the CAPT simulations, we conducted three 5-year Atmospheric Model Intercomparison Project (AMIP)-style simulations with present-day forcing for year 2000 from the IPCC AR5 emission dataset. The sea surface temperature (SST) and sea ice are prescribed from the observed climatological annual cycle. The land model is from the Community Land Model version 4.5 with a few additional developments. The three AMIP simulations have the same model settings as the CAPT simulations in terms of the model grids (ne30 vs. CONUS RRM) and the physical tuning parameters with CONUS RRM grids (ne30 vs. ne120 tuning parameters; see Table 1 for details). Since the first year of these simulations involve model spin-up behaviors, we only analyze the last 4 years of these simulations.

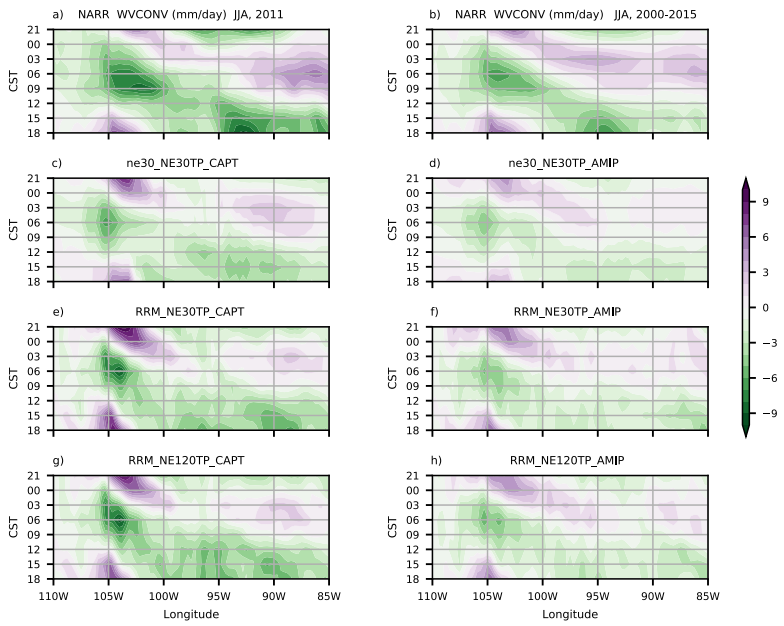

Figure 13. Hovmöller diagrams (35°N-45°N) of the NARR JJA moisture convergence over the time period **(a)** 2011, and **(b)** 2000-2015; the Day2 output of the EAM1 CAPT simulations for 2011: **(c)** ne30_NE30TP_CAPT, **(e)** RRM_NE30TP_CAPT, and **(g)** RRM_NE120TP_CAPT; and the EAMv1 5-year AMIP runs: **(d)** ne30_NE30TP_AMIP, **(f)** RRM_NE30TP_AMIP, and **(h)** RRM_NE120TP_AMIP. The y-axis is the Central Standard Time (CST).

Our study regarding the summertime precipitation bias, and its relationship with the convection scheme and the large-scale environment has been summarized in Zheng et al. (2019):

i. EAMv1 tends to generate a wet seasonal mean precipitation bias over the Rockies and a dry bias over the Great Plains during the summertime (Figure 12). Because the model fails to capture strong precipitation events associated with MCSs that often occur over the Great Plains, the current model tuning practice, which either increases or decreases the amount of convective precipitation, cannot simultaneously reduce the precipitation bias over the Great Plains and the Rocky Mountain region.

ii. The lack of eastward propagation of precipitation and the resulting dry bias over the Great Plains is related to the boundary layer at the western edge of the bias area being too dry. The meridional moisture transport at the southern edge of the central US being too weak is one of the causes. Although the study cannot clarify the causes of the too dry boundary layer and the too weak moisture transport, the sensitivity test on the tuning parameters indicate the clear impact of the ZM scheme on the large-scale moisture transport.

iii. Because the ZM scheme contributes the bulk of the precipitation, it also controls its diurnal cycle. The ZM convective precipitation does not respond to the increase of the moisture convergence as the NARR precipitation does. Therefore, even though EAMv1 can generally capture the eastward propagation of the moisture convergence starting at the eastern edge of the Rockies and the moisture divergence that follows the convergence (Figure 13), and it generates the eastward propagation of large-scale upward motion, the precipitation still becomes out-of-phase with the moisture convergence east of 100°W and develops a biased diurnal cycle (Figure 14).

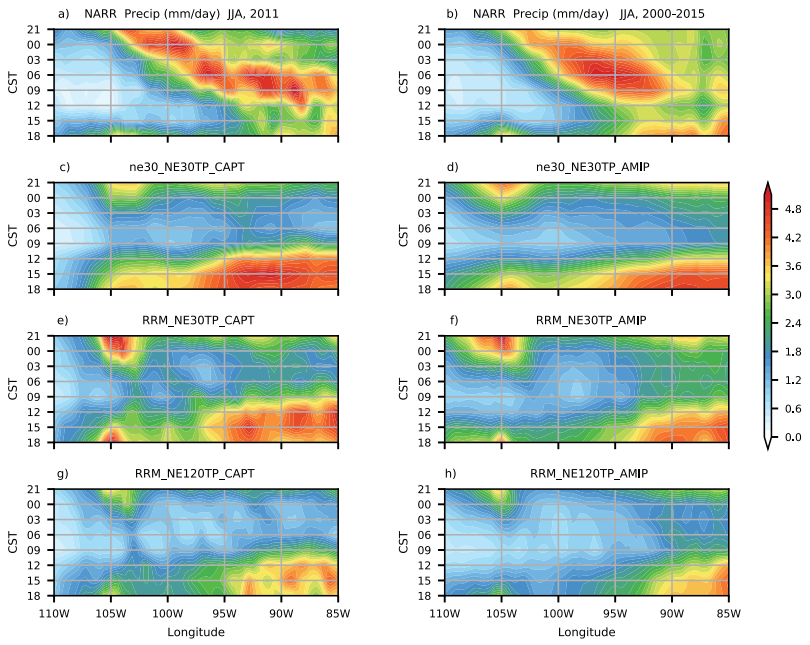

Figure 14. Hovmöller diagrams (35°N-45°N) of the JJA precipitation rate (unit: mm/day) from the NARR data over the time period **(a)** 2011, and **(b)** 2000-2015. The Day2 output from the EAMv1 CAPT simulations for the year 2011: **(c)** ne30_NE30TP_CAPT, **(e)** RRM_NE30TP_CAPT, and **(g)** RRM_NE120TP_CAPT. The Hovmöller diagrams (35°N-45°N) of the JJA precipitation rate (mm/day) from the EAMv1 5-year AMIP runs: **(d)** ne30_NE30TP_AMIP, **(f)** RRM_NE30TP_AMIP, and **(h)** RRM_NE120TP_AMIP. The y-axis is the Central Standard Time (CST).

These results confirmed that the ZM convection scheme is the major source of the precipitation diurnal cycle bias over the Great Plains, and the main contributor to the dipole in precipitation bias between the Rockies and the Great Plains. The ZM convection scheme also clearly impacts the moisture flux transport over the central US. This study served as motivation for exploring alternate treatments of triggering in E3SMv1 to make its convection more responsive to the large-scale environment, less constrained to the local surface heating, and more capable of representing long-lasting MCSs (see Section 5.1). Furthermore, the model diagnostics in this study can help track model performance of the controlling factors on the summertime precipitation over this region as model resolution increases and physical schemes are updated. To do so, we are planning to incorporate some of these diagnostics into E3SM Diags.

4.3 Elevated convection

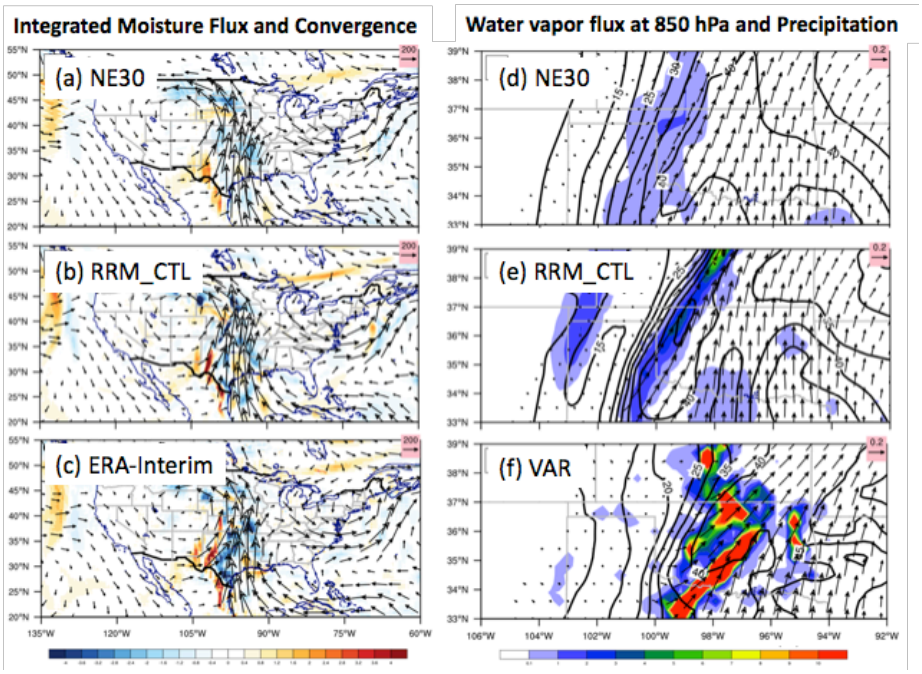

Figure 15. (a) to (c): Vertical integrated moisture flux (kg/m/s) and flux convergence (mm/hour) in NE30, RRM_CTL and ERA-Interim. (d)-(f) Moisture flux at 850 hPa (m/s) and precipitation in NE30, RRM_CTL, and 3D-ARM-VAR. The time is 12Z May 20, 2011.

SBU also analyzed the E3SM simulations described in the previous section (4.2) in combination with the newly developed 3D-ARM-VAR dataset (Section 3.1). We studied the cause of the deficient precipitation over the ARM SGP domain in the E3SM NE30 and E3SM RRM_CTL CAPT simulations for the MC3E event. The CAPT simulations in NE30 and RRM_CTL simulated well the large-scale circulation of the observed cyclone over the SGP and the enhanced northward transport of moisture to the east of the cyclone. This is shown in Figure

15(a)-(c) that compares the vertically integrated moisture flux (vector) and convergence (color) in NE30 and RRM_CTL with those from ERA-Interim. The models however failed to simulate the observed strong rainfall over the SGP as shown in the zoomed-in Figure 15(d)-(f), especially in NE30, which was not accurately captured either in the ERA-Interim.

We found that the model barely triggered convection over the SGP during the event. The 3D-ARM-VAR analysis showed that the maximum moist static energy is elevated above the atmospheric boundary layer. This is captured in E3SM NE30 and RRM_CTL as shown in Figure 16(a)-(c) in the zonal-vertical cross section of moist static energy in NE30 and RRM_CTL and the VAR analysis. VAR indicated vertical mixing of the moist static energy in this elevated region, but in NE30 and RRM_CTL, convection is not triggered because the moist static energy in the boundary layer is not large enough. We therefore concluded that the launch level of deep convection in the model needs to be revised to allow elevated convection, and this is why the models do not simulate precipitation over the SGP during the event. This finding served as additional motivation for revisiting convective triggering in E3SM (see Section 5.1)

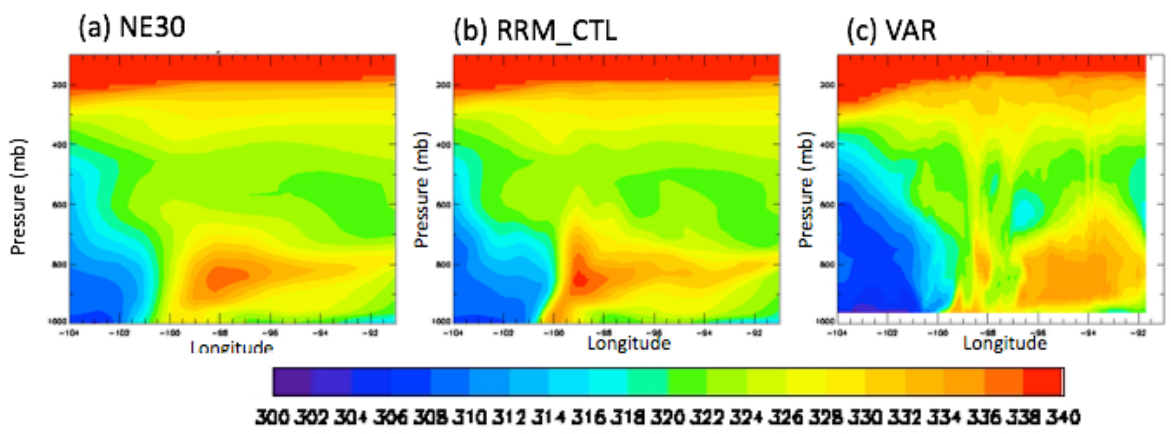

Figure 16. (a) to (c): Longitude-pressure cross section of moist static energy at the SGP Central Facility latitude in NE30, RRM_CTL, and VAR. The time is 12Z May 20, 2011.The x-axis is from104°W to 91°W. The unit has been converted to Kelvin degree.

4.4 TWP CRM Simulations and analysis

Global models like E3SM are still far from being able to explicitly resolve convective processes. With the regional refinement capability, E3SM could theoretically offer global coverage with regions of interest refined to study the model behavior at very high resolution and to focus cloud processes. With such future high-resolution E3SM applications in mind, we performed convection-permitting simulations to analyze the scale dependency and gauge the need for subgrid parameterization as model grid resolution increases.

The active monsoon period during the TWP-ICE field campaign was simulated using WRF at a 1 km grid resolution. We use the same enhanced WRF model that is used for LASSO simulations, which was developed in a previously supported DOE project. The scale dependency of convective properties is analyzed using a spatial filter for scale separation. Figure 17 shows the vertical transport of liquid potential temperature and total water fluxes, partitioned into contributions by resolved and subgrid scales. It can be seen that while the contribution from the resolved flow clearly increases as the grid size decreases, even at 5 km grid resolution nearly over half of the transport is still contributed by subgrid scale motions. This subgrid component would have to be parameterized in E3SM RRM configurations at this resolution.

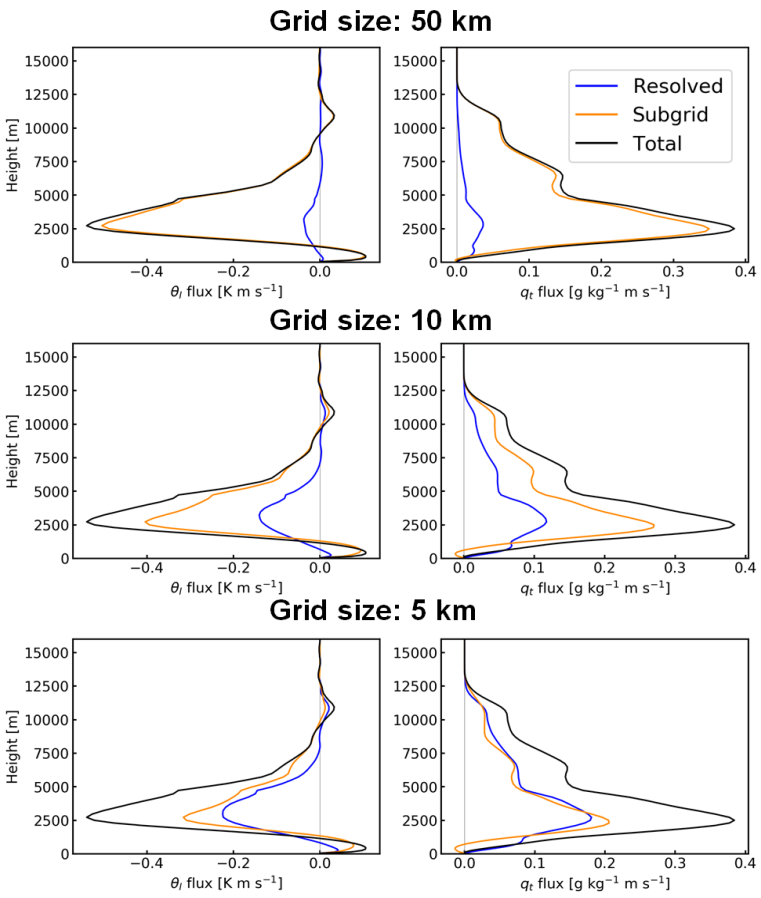

Figure 17. The partition of the vertical transport of liquid water potential temperature **(left)** and total water **(right)** by equivalent grid sizes.

4.5 Validating E3SMv1 at TWP

In order to conduct an initial comparison of E3SM against the CPOL observations, E3SM was run at 1-degree resolution and was nudged with ERA-Interim forcing. This run spans the years 2009 to 2011. This, in total, creates for 4 grid boxes in the E3SM that overlap with the CPOL radar's coverage for the 2-year period. Therefore 3 hourly rainfall accumulations over these 4 grid boxes were estimated from the CPOL data and compared against the 3 hourly accumulations from E3SM. Figure 18 shows the p.d.f. of these 3 hourly accumulations as a function of time of day for one of these boxes. Figure 18 shows that, in general, E3SM produces too many periods of rainfall rates less than 1 mm/hr while the CPOL observations show a clear afternoon peak of rainfall rates > 1 mm/hr. This shows that E3SM is not correctly resolving the diurnal cycle of precipitation over Darwin. Analyses of the other 3 boxes showed similar results (not shown). This lack of skill of this run of E3SM in resolving the diurnal cycle could be due to the coarse run resolution preventing the dynamical core from being able to generate seabreezes. The simplistic assumptions made by the convective trigger that triggers convection when CAPE is above a certain threshold may also be inadequate for properly triggering diurnal convection. These findings served as additional motivation for the revised convective triggers in Sections 5.1 and 5.2.

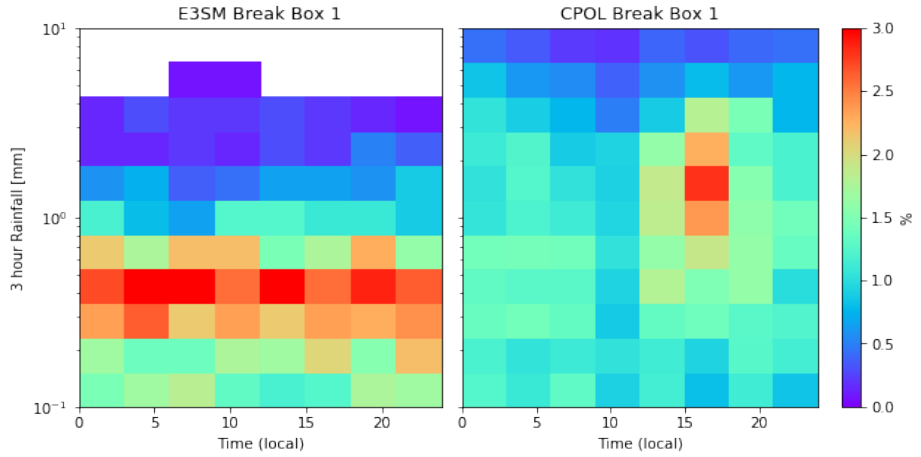

Figure 18. (Left) p.d.f.s of 3 hourly accumulations from a grid box of E3SM over the Darwin region. **(Right)** the 3 hourly accumulations averaged over the same grid box, but from CPOL.

Additional E3SM simulations to investigate the impact of these improvements to the representation of the diurnal cycle in Darwin have been discussed but not carried out yet due to a lack of time. Performing runs with the RRM grid, increased resolution, and with the newly proposed triggers, including the new machine learning based convective trigger are future works that have been motivated by the CMDV-RRM project. Without the close collaboration of modelers and observationalists that was the defining characteristic of CMDV, such guidance would have been difficult to devise.

4.6 Validating E3SMv1 with CAPT simulations with ENA RRM

The purpose of the ENA RRM grid is to aid in understanding high resolution model behavior over the ARM ENA site (Figure 3). A large diversity of marine boundary layer cloud conditions including winter frontal stratus clouds, stratocumulus and trade wind cumulus clouds exist at this site. These cloud systems are susceptible to aerosols. We conducted and analyzed CAPT simulations with ENA RRM and ne30 (1 degree) during the ARM CAP-MBL field campaign (June 2009 to December 2010). With ARM cloud observations, we can evaluate the cloud processes simulated by E3SMv1 (Figure 19). We will share the simulations with Virendra Ghate at Argonne National Laboratory to continue the model assessment and better understand:

a. the impacts of vertical and horizontal resolution on the representation of drizzling MBL clouds.

b. the relevance of the process-level differences among the different grids to the modeled climate state.

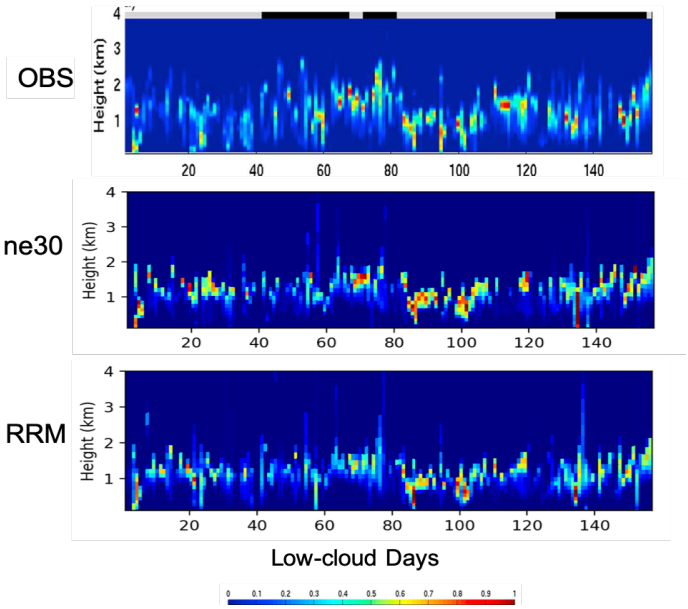

Figure 19. Daily cloud fraction from **(top)** the observations, **(middle)** E3SM ne30, and **(bottom)** E3SM ENA RRM during MBL cloud days. Alternating gray bars and black bars along the panels indicate days during June, July and August (JJA) 2009, September, October and November (SON) 2009, December, January and February (DJF) 2010, March, April and May (MAM) 2010, JJA 2010, SON 2010, and December 2010.

5 Model development

5.1 Revised convection trigger

As demonstrated in Sections 4.2, 4.3, and 4.4, E3SMv1 as well as most current weather and climate models continue having difficulties in modeling the diurnal variation in precipitation. Over land, most models tend to rain too early after sunrise with a rainfall maximum around the local noon rather than the observed late afternoon peak and fail to capture the observed nocturnal peak (e.g. Dai, 2006). Over ocean, the diurnal cycle in most models is weak with peaks around 0200 local solar time (LST) compared to 0400–0600 LST in the observations. In general, models often rain too frequently at reduced intensity. Increasing model horizontal resolution seems to help slightly improve rainfall intensity, but it has little impact on the phase of the diurnal cycle of precipitation (e.g. Tang *et al.*, 2019).

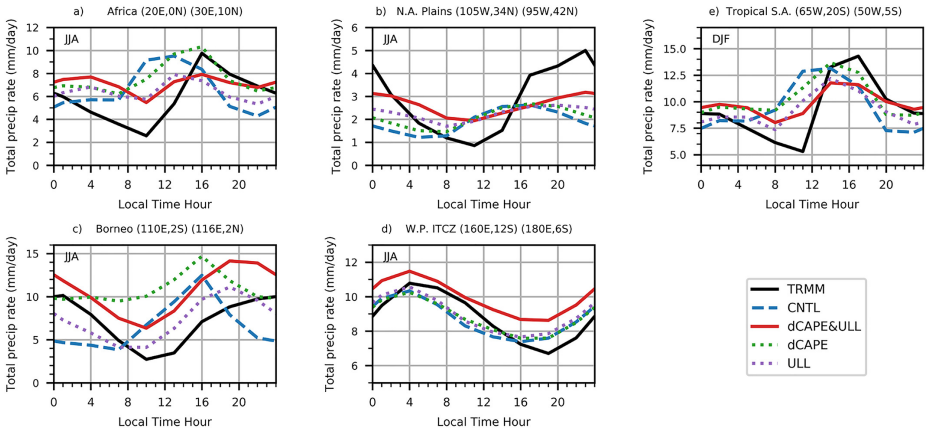

Figure 20. Diurnal cycle of precipitation over: **(a)** tropical North Africa (JJA), **(b)** North America Plains (JJA), **(c)** central Borneo Island (JJA), **(d)** western Pacific ITCZ (JJA), and **(e)** tropical South America (December-January-February, DJF), from TRMM (black) and models: CNTL (blue), dCAPE&ULL (red), dCAPE (green), and ULL (purple).

Earlier studies highlighted that deficiencies in representing moist convection processes, in particular convection initiation, could largely account for the failure in capturing the diurnal cycle of precipitation in climate models (Dai & Trenberth, 2004). We proposed a new convective triggering mechanism to improve the E3SM capability to modeling the diurnal cycle of precipitation. The new convective triggering mechanism uses a dynamic constraint, referred to as the dynamic Convective Available Potential Energy (dCAPE), for preconditioning of the convection-favoring environment and to prevent CAPE from being released spontaneously, and it adopts the Unrestricted air parcel Launch Level (ULL) scheme to capture elevated convection. With the new convective triggering mechanism, E3SM shows dramatic improvements in capturing the timing of rainfall events over both midlatitude and tropical lands (Figure 20). The nocturnal peak of precipitation and the eastward propagation of convection downstream of the Rockies and

over the adjacent Great Plains are also much better captured than those in the default model (Figure 21). It is one of a very few models that can capture the nocturnal elevated convection. The improvements represent an important advance in modeling the diurnal cycle of precipitation. This study has been published on *Journal of Advances in Modeling Earth Systems* (Xie et al., 2019) and highlighted on the Eos Research Spotlight (Shultz, 2019).

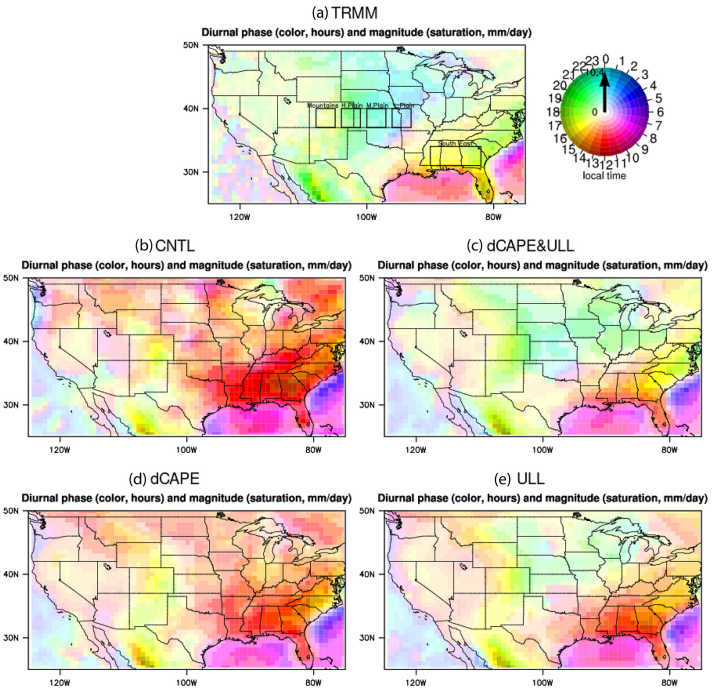

Figure 21. Timing phase (color) and amplitude (color density) of the first diurnal harmonic of total precipitation (mm/day) over CONUS during JJA from 10 years of 3-hourly averaged data for **(a)** TRMM, **(b)** CNTL, **(c)** dCAPE&ULL, (**d**) dCAPE, and **(e)** ULL.

5.2 A machine learning-based deep convective trigger

As previously discussed, convective triggering remains a major weakness in the deep convective parameterization used in the E3SMv1, which affects the simulated precipitation characteristics and many other regional and global features. Tackling convective triggering to improve the model performance, specifically for diurnal precipitation, was one subtask of the CMDV-RRM project. In addition to a conventional approach undertaken by our project team to account for destabilization due to dynamical and thermodynamical processes to improve the diurnal simulation (Section 5.1), a trigger function based on machine learning is also developed by BNL. This novel trigger function uses the classification model XGBoost, a highly efficient and scalable tree-based gradient boosting model. It is trained and tested using long-term constrained variational analysis forcing data from the ARM SGP and GoAmazon (see Table 2 for the variables used by XGBoost). Convective events are defined by an hourly precipitation rate exceeding 0.5

mm/hour, as used in Suhas and Zhang (2014) for SGP in summer time and GoAmazon year-round. Table 3 gives a comparison of the performance with other conventional approaches for SGP and GoAmazon data that are trained and tested separately. The performance score shown in Table 3 is a harmonic mean of recall and precision for both the convective and non-convective events. Clearly the XGBoost ensemble classification algorithm substantially outperforms the conventional convective trigger functions, including the better ones identified in Suhas and Zhang (2014). Training and testing using the joint SGP/GoAmazon data has also been performed to achieve a comparable high-performance score.

Table 2. Variables used in machine learning

Single level	Latent heat flux
	Sensible heat flux
	Air temperature at the surface
	Air relative humidity at the surface
	Convective available potential energy
	Lifting condensation level
Vertical Profiles below 100 mb	Temperature (T)
	Specific humidity (Q)
	Horiz. advective tendency of T
	Horiz. Advective tendency of Q

Table 3. Comparison of performance scores

Method	SGP Score	Amazon Score
XGboost	0.94	0.86*
Dilute cape	0.62	0.42
Dilute dcape	0.71	0.46
Undilute cape	0.27	0.21
Undilute dcape	0.35	0.22

6 Tools

6.1 StrideSearch

Given our primary focus on improving the understanding of clouds, precipitation, and convection in E3SM over ARM sites using observational data, SNL also sought to develop a storm-finding and tracking tool that would work for global model output. We developed this capability from the StrideSearch tool[3].

An objective was to find and track mesoscale convective storms (MCSs). MCSs are minimally resolved in E3SM and reanalysis output given their size of approximately 100km and the E3SM 1/4-degree resolution of 25 km. StrideSearch had been developed to look for larger extratropical cyclones with approximately 1000km horizontal footprint. If output was remapped from the E3SM native grid output, i.e., unstructured regionally refined cubed sphere meshes, to structured latitudinal-longitudinal grids, information about the storms would be lost in the regridding processes. Thus, instead of searching for storms on exclusively latitudinal-longitudinal cartesian grids, StrideSearch was further developed to incorporate a kd-tree algorithm to search for mesoscale convective systems. K-dimensional trees (kd-trees) are built to describe relationships between points. Figure 22 shows the objective of this development to speed-up the analysis workflow. Using k-d trees allows us to handle unstructured data without conversion.

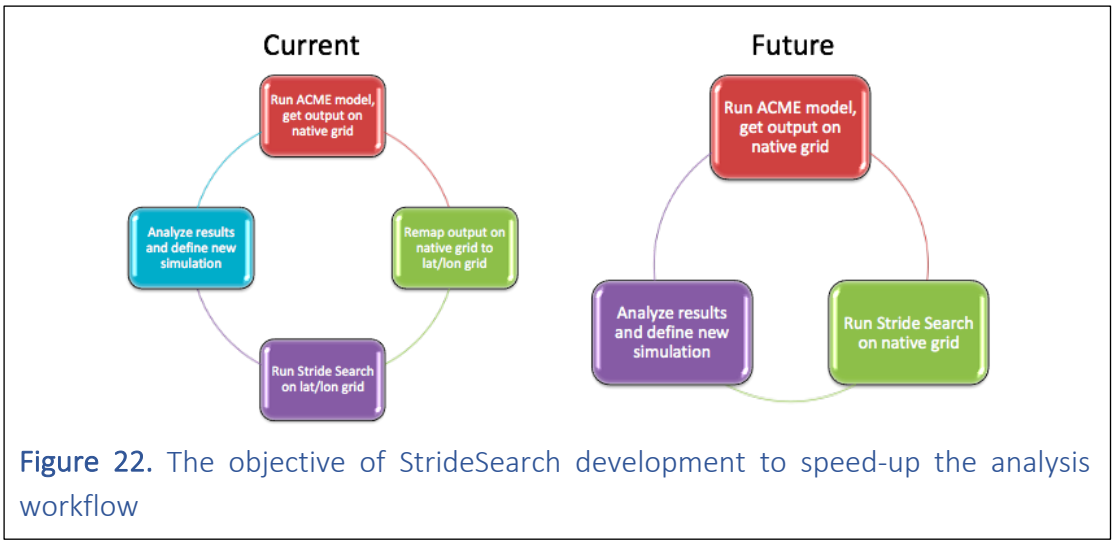

Figure 22. The objective of StrideSearch development to speed-up the analysis workflow

Figure 23 shows how the data is organized from a simulation using RRM grid, such as CONUS (left), and how StrideSearch would search for storms within the dataset within each circle (blue, then red, then black) for 3 compared resolutions.

[3] https://github.com/pbosler/StrideSearch

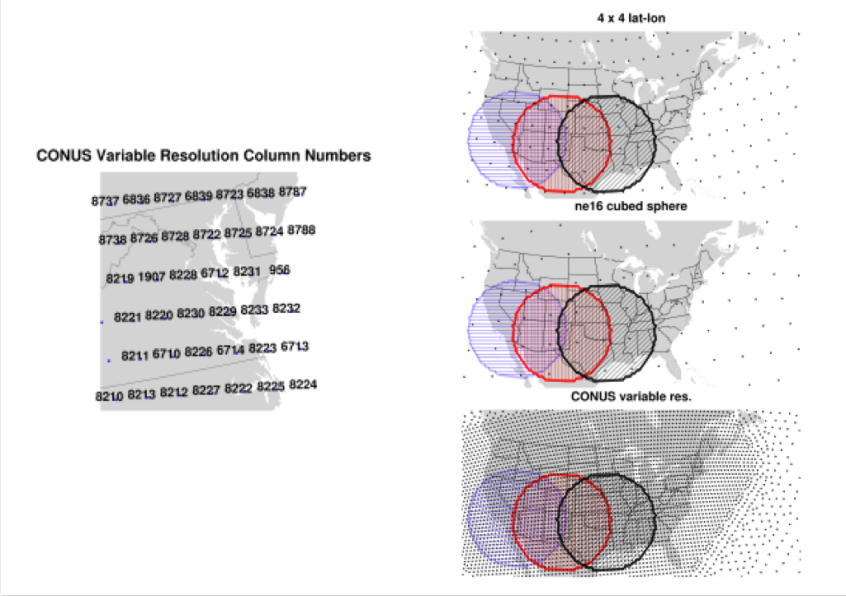

Figure 23. (Left) CONUS variable resolution column numbers, and (right) how StrideSearch would search for storms within the dataset within each circle (blue, then red, then black) for 4x4, ne16 and CONUS RRM.

6.2 PyDDA

As part of the retrieval of the 3D wind fields from the CPOL data, ANL developed a scalable multiple Doppler retrieval package that can be applied to the data. While Multidop was available for use as a wind retrieval package that was able to ingest Cf-Radial CPOL data, this package is not scalable to datasets as large as CPOL's. This therefore motivated us to develop PyDDA, a new multiple Doppler retrieval package written entirely in Python. PyDDA is publicly available[4] allowing anyone in the scientific community to use it.

6.3 TINT Is Not TITAN: TINT

This project also supported the development of TINT Is Not TITAN (TINT) package. TINT package works directly with the Py-ART grid object in Python and is based on the Thunderstorm Identification, Tracking, Analysis and Nowcasting package (TITAN; Dixon and Wiener, 1993). While TITAN was designed to be used in operational settings and can be challenging to configure, TINT is designed to simply take a temporal sequence of grids, a function that renders the 3-D grids to a 2-D binary mask (for example, a reflectivity threshold at a single level) denoting cell or no cell and returns a Pandas (McKinney, 2010) data frame containing cell locations and characteristics as a function of time. TINT does not deal with splits or mergers but is thread-safe

[4] https://openradarscience.org/PyDDA

and pleasantly parallel when radar data are stratified by storm events (Figure 24). The peak in the cross-correlation gives a good indication of the image shift between the two time-steps and is used as the position start of the search to identify cells in subsequent images. TINT is described in detail in a recent paper (Fridlind et al 2019) where it was also used to inform a proposal to deploy the ARM Mobile Facility to Houston, Texas. TINT is available as community code[5].

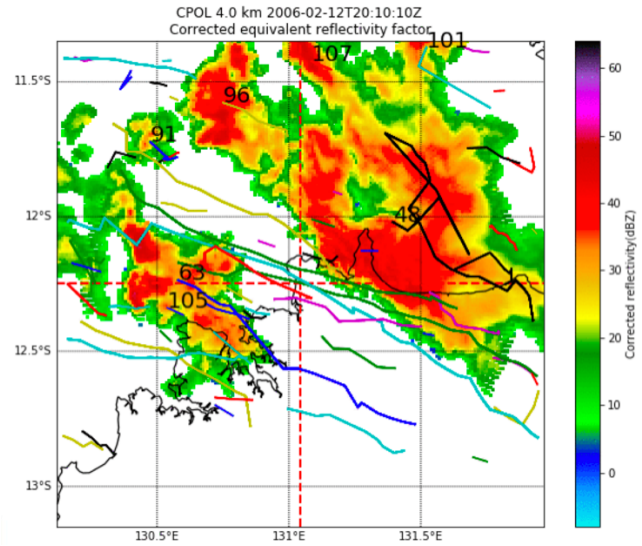

Figure 24. Reflectivity factor from CPOL at 4km and associated cell tracks retrieved by TINT. TINT is very robust but can have issues with splits and mergers as seen in cell track 48 above.

6.4 Multi-Objective Optimization Framework

BNL developed a constrained multi-objective optimization (MOO) framework aimed to be used for obtaining a more consistent tuning for E3SM low- and high-resolution atmosphere models. This work consists of two major steps. Under the support of CMDV-RRM, we finalized the previous development of a single objective optimization framework for exploring the feasibility of automatic optimization of parameters in the GCM's physical parameterizations (Zhang et al. 2018). The auto-optimization framework uses short-term, CAPT-like hindcast simulations and an improved downhill simplex optimization algorithm (Zhang et al. 2015). When applied to the well-calibrated CAM5, a 10% reduction of overall biases is found based on predefined metrics that account for model biases in precipitation, temperature, and humidity as well as in longwave and shortwave cloud radiative forcing fields.

[5] https://github.com/openradar/TINT

The MOO framework builds on this one-objective framework to include both low-resolution and high-resolution models as optimization objectives. In the current design, it has three objectives. Regional metrics from the standard EAM low-resolution configuration is the primary optimization objective, and high-resolution model metrics from the same region (represented by RRM both as a demonstration and for computational efficiency), and global metrics from the low-resolution model are used as constraints (see Table 4). RRM over TWP is selected to represent a high-resolution configuration over the convectively active tropical region that are most sensitive to tunings adopted for EAMv1 that are different for low- and high-resolution models.

Table 4. Structure of the constrained multi-objective optimization framework

Objective	Type	Region	Resolution	Basis of metrics (justified by analysis)
1	optimization	TWP	1°	Performance score for: PRECT, LWCF, SWCF, CLDLOW, CLDMED, CLDHGH, PRECT pdf
2	constraint	TWP	RRM 0.25° to 1°	Same as 1
3	constraint	Global	1°	Performance score for: PRECT, LWCF, SWCF, Q850

In practice, a 2-stage tuning strategy is further adopted to speed up the auto-tuning process.

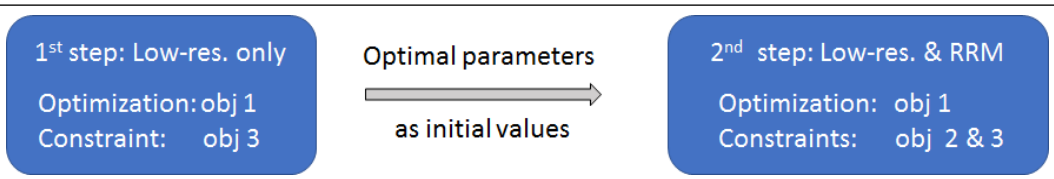

Figure 25. Diagram of the two-stage MOO workflow

The full workflow has been applied to the EAMv1 for an experimental auto-tuning to re-tune a total of 8 parameters in deep convective, CLUBB, and microphysical schemes that use different values in the current low- and high-resolution EAMv1. With a limited number of iterations, the algorithms are able to find common tunings for the 8 parameters that improve the simulation metrics for both low- and high-resolution models for the region of interest (TWP-RRM) as well as for low-resolution model at global scale (Figure 25). In the figure, the numbers are for the combined metrics (Table 2) for low-resolution simulations over the TWP and the globe, and a high-resolution RRM simulation over the TWP. A value smaller than 1 indicates improvement over standard EAMv1 configuration. Note that the algorithm uses a localized optimization and the iterations are not required to move in one fixed direction in terms of metric criterion. The best performing parameter choices are selected from the full iteration pool. The 2nd stage requires 3 sets of parameter choices from the 1st stage in this 3-objective framework. It is shown that improved tunings can be found during the 1st stage (Figure 26), with further improvements

achievable in stage 2. Continued exploration of a common tuning for EAM low-res and high-res models is underway using this MOO framework and the RRM meshes developed under this project. The full MOO software along with documentation has been published on GitHub[6].

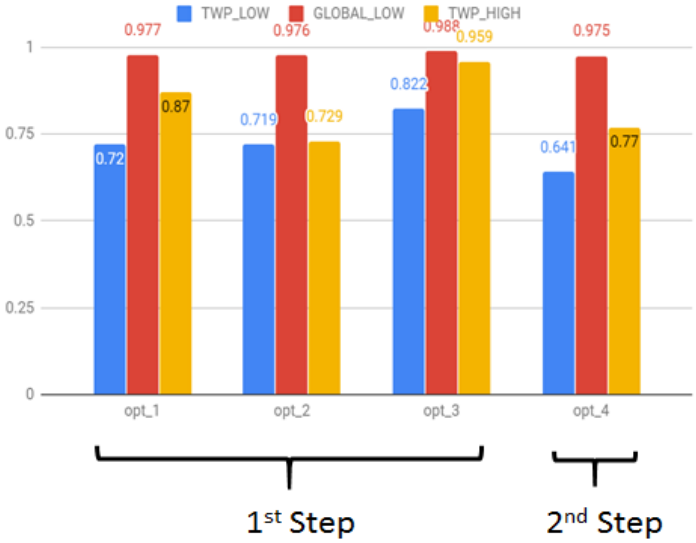

Figure 26. Optimal overall performance scores from the two-step workflow after 91 iterations for step 1 and 8 iterations for step 2. A score <1 means improvement over default.

[6] https://github.com/eexcalibur/GCM_paras_tune

7 Synthesis

This project intentionally assembled a set of scientists with varied backgrounds and perspectives: observations, data analysis, process-level and model development. Rather than trying to adhere to a compartmentalized set of tasks and deliverables, we tried to develop an open and respectful culture with active interactions between project members and opportunities to redirect priorities based on where the science was leading us. Most of the deliverables in this project have been positively impacted by that culture. Figure 27 summarizes key project interactions and impact of the deliverables beyond the project itself.

The design of the new RRM grids for TWP and ENA resulted from a number of back-and-forth discussions between observationalists and model developers to maximize the usefulness of future model simulations, while staying within computational constraints. Both TWP and ENA grids will likely find users beyond this project, in particular for evaluating E3SM against ASR data. Indeed, Virendra Ghate at ANL has already expressed interest in further analyzing available E3SM ENA RRM simulations.

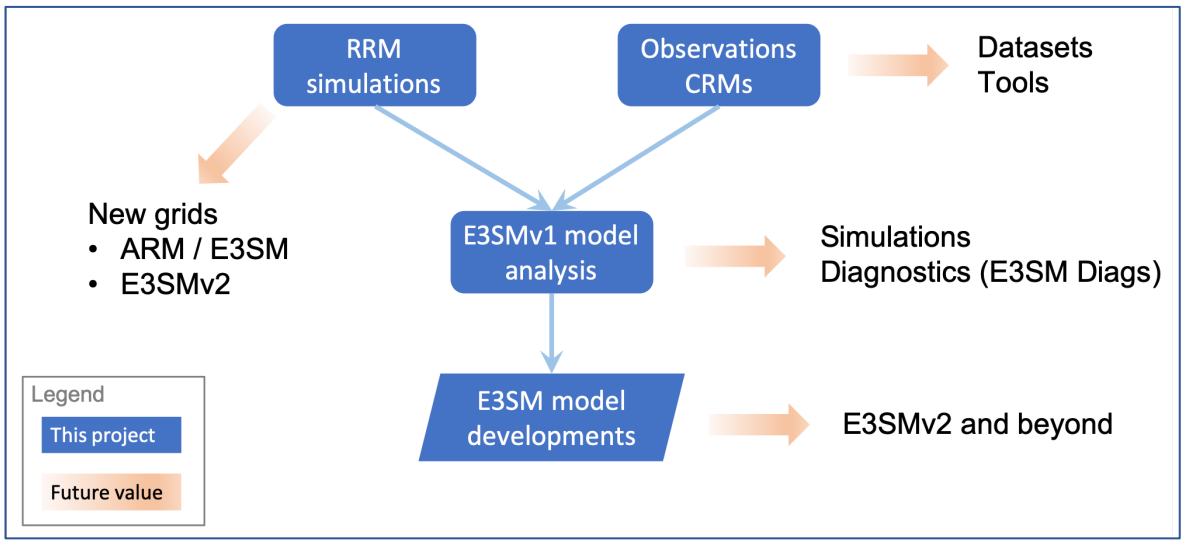

Figure 27. Schematic of active interactions within the project and impact of deliverables beyond the project.

Parameterized deep convection, and in particular the trigger mechanisms, emerged through the project as a focal point from three separate lines of investigations.

Analysis of E3SM CONUS simulations unsurprisingly revealed the inability of the model to simulate propagating convection over the central US (Figures 12, 14). However, and surprisingly, E3SM is capable of simulating the propagation of moisture convergence/divergence patterns

(Figure 13). This pointed the finger squarely at the ZM deep convection and its inability to properly respond to large-scale forcing.

At the same time, analysis of the same simulations but focusing on a specific MC3E case-study (May 20, 2011) revealed that E3SM failed to properly simulate observed precipitation because the ZM convection is incapable of generating elevated convection (Figure 16).

In the tropics, comparison of E3SM 3-hourly rainfall accumulation with newly derived CPOL data also revealed problems with the diurnal cycle of precipitation. E3SM produces too many periods of rainfall rates less than 1 mm/hr while the CPOL observations show a clear afternoon peak of rainfall rates > 1 mm/hr (Figure 18). Again, this is related to simplistic assumptions made by the convective trigger that triggers convection when CAPE is above a certain threshold.

These findings motivated S. Xie and collaborators to revisit ideas on how to improve convective triggering. Two modifications were explored. The first one uses a dynamic constraint, referred to as the dynamic Convective Available Potential Energy (dCAPE), for preconditioning the convection-favoring environment and preventing CAPE from being released spontaneously as is the case in traditional CAPE closures. The second modification implements the Unrestricted air parcel Launch Level (ULL) scheme to capture elevated convection.

With these changes, E3SM shows dramatic improvements in capturing the timing of rainfall events. It now is one of very few models that can capture the nocturnal elevated convection. The improvements (Figures 20, 21) represent an important advance in modeling the diurnal cycle of precipitation. The resulting publication (Xie et al. 2019) was selected by EOS for a highlight. These modifications are high on the priority list for incorporation in the next version of E3SM.

8 Lessons learned

- Bringing developers from the E3SM community together with boots-on-the-ground observationalists has helped develop a better sense (for all) of model and observational constraints. Subject matter experts of physical processes shared domain knowledge freely over the course of the project.
- We recommend that BER consider funding similar activities in the future. In particular, closer collaborations between ASR and E3SM scientists would be mutually beneficial.
- It takes a while to develop such interactions and three years is a relatively short timeframe. One option to consider would be to offer extensions for future successful projects, in order to keep existing teams in place but extend the science.
- Although an adjustment period was needed at the beginning of the project to conceive a smaller and coherent project from a subset of tasks, we found that a smaller team allowed us to develop more active interactions focused around a signature capability, the RRM.
- This project highlighted the need to simplify the process of generating RRM grids and supporting model input datasets. Knowledge from this team has been transferred to E3SM and the E3SM project is now actively stream-lining the grid generation process.
- Given that numerical convergence tests are not generally performed due to computational expense in earth system science, we are finding the RRM utility appears to be a good way to test convergence of model properties and scale-awareness.

9 Appendix: deliverables

9.1 Journal articles (CMDV team members in bold)

9.1.1 Published or Accepted

1. Lin., Y., W. Dong, **M. Zhang**, Y. Xie, W. Xue, J. Huang, and Y. Luo, 2017: Causes of model dry and warm bias over central U.S. and impact on climate projections. Nature Communications 8, Article number: 881(2017), https://doi.org/10.1038/s41467-017-01040-2
2. Chen, J., Liu, Y., **Zhang, M.**, & Peng, Y. (2018). Height dependency of aerosol-cloud interaction regimes. Journal of Geophysical Research: Atmospheres, 123, 491–506, https://doi.org/10.1002/2017JD027431
3. Yu, H. Y., and **M. H. Zhang**, 2018: Explaining the year-to-year variability of the eastern Pacific intertropical convergence zone in the boreal spring. *J. Geophys. Res. Atmos.*, https://doi.org/10.1002/2017JD028156
4. Chen, J., Liu, Y., **Zhang, M**., & Peng, Y., 2018: Height dependency of aerosol-cloud interaction regimes. Journal of Geophysical Research: Atmospheres, 123. https://doi.org/10.1002/2017JD027431
5. **Xie, S.**, **W. Lin**, P. J. Rasch, P.-L. Ma, R. Neale, V. E. Larson, Y. Qian, P. A. Bogenschutz, P. Caldwell, P. Cameron-Smith, **J.-C. Golaz**, S. Mahajan, B. Singh, Q. Tang, H. Wang, J.-H. Yoon, K. Zhang, Y. Zhang, 2018: Understanding Cloud and Convective Characteristics in Version 1 of the E3SM Atmosphere Model. *JAMES,* https://doi.org/10.1029/2018MS001350
6. Louf, V., A. Protat, R. A. Warren**, S. M. Collis,** D. B. Wolff, S. Raunyiar, C. Jakob, W. A. Petersen, An integrated approach to weather radar calibration and monitoring using ground clutter and satellite comparisons, Journal of Atmospheric and Oceanic Technology, 36, 17-39, 2019, https://doi.org/10.1175/JTECH-D-18-0007.1
7. **Jackson, R. C.**, **Collis, S. M.**, Louf, V., Protat, A., and Majewski, L.: A 17 year climatology of the macrophysical properties of convection in Darwin, *Atmos. Chem. Phys.*, 18, 17687-17704, https://doi.org/10.5194/acp-18-17687-2018, 2018.
8. Fridlind, A. M., van Lier-Walqui, M., **Collis, S**., Giangrande, S. E., **Jackson, R. C.**, Li, X., Matsui, T., Orville, R., **Picel, M. H**., Rosenfeld, D., Ryzhkov, A., Weitz, R., and Zhang, P.: Use of polarimetric radar measurements to constrain simulated convective cell evolution: a pilot study with Lagrangian tracking, Atmos. Meas. Tech., 12, 2979-3000, https://doi.org/10.5194/amt-12-2979-2019, 2019.
9. **Tao Zhang**, **Minghua Zhang**, **Wuyin Lin**, Yanluan Lin, Wei Xue, Haiyang Yu, Juanxiong He, Xiaoge Xin, Hsi-Yen Ma, **Shaocheng Xie**, Weimin Zheng 2018: Automatic tuning of the Community Atmospheric Model (CAM5) by using short-term hindcasts with an improved downhill simplex optimization method, *Geosci. Model Dev.*, 11, 5189-5201, https://doi.org/10.5194/gmd-11-5189-2018

10. **J.-C. Golaz**, P. M. Caldwell, L. P. Van Roekel, M. R. Petersen, Q. Tang, J. D. Wolfe, G. Abeshu, V. Anantharaj, X. S. Asay-Davis, D. C. Bader, S. A. Baldwin, G. Bisht, P. A. Bogenschutz, M. Branstetter, M. A. Brunke, S. R. Brus, S. M. Burrows, P. J. Cameron-Smith, A. S. Donahue, M. Deakin, R. C. Easter, K. J. Evans, Y. Feng, M. Flanner, J. G. Foucar, J. G. Fyke, B. M. Griffin, C. Hannay, B. E. Harrop, E. C. Hunke, R. L. Jacob, D. W. Jacobsen, N. Jeffery, P. W. Jones, N. D. Keen, S. A. Klein, V. E. Larson, L. R. Leung, H.-Y. Li, **W. Lin**, W. H. Lipscomb, P.-L. Ma, S. Mahajan, M. E. Maltrud, A. Mametjanov, J. L. McClean, R. B. McCoy, R. B. Neale, S. F. Price, Y. Qian, P. J. Rasch, J.E.J. Reeves Eyre, W. J. Riley, T, D. Ringler, A. F. Roberts, **E. L. Roesler**, A. G. Salinger, Z. Shaheen, X. Shi, B. Singh, J. Tang, M. A. Taylor, P. E. Thornton, A. K. Turner, M. Veneziani, H. Wan, H. Wang, S. Wang, D. N. Williams, P. J. Wolfram, P. H. Worley, **S. Xie**, Y. Yang, J.-H. Yoon, M. D. Zelinka, C. S. Zender, X. Zeng, **C. Zhang**, K. Zhang, Y. Zhang, **X. Zheng**, T. Zhou, Q. Zhu, 2019: The DOE E3SM coupled model version 1: Overview and evaluation at standard resolution, *JAMES*, https://doi.org/10.1029/2018MS001603.
11. **S. Xie**, Y.-C. Wang, **W. Lin**, H.-Y. Ma, Q. Tang, S. Tang, **X. Zheng**, **J.-C. Golaz**, G. Zhang, **M. Zhang**: Improved diurnal cycle of precipitation in E3SM with a revised convective triggering function, *JAMES*, https://doi.org/10.1029/2019MS001702.
12. Q. Tang, S. A. Klein, **S. Xie**, **W. Lin**, **J.-C. Golaz**, **E. L. Roesler**, M. A. Taylor, P. J. Rasch, D. C. Bader, L. K. Berg, P. Caldwell, S. E. Giangrande, R. Neale, Y. Qian, L. D. Riihimaki, C. S. Zender, Y. Zhang, and **X. Zheng**, 2019: Regionally refined test bed in E3SM atmosphere model version 1 (EAMv1) and applications for high-resolution modeling. *Geosci. Model Dev.*, 12, 1–28, https://doi.org/10.5194/gmd-12-1-2019.
13. **R. Jackson, S. Collis,** T. Lang, C. Potvin, and T. Munson, 2019: PyDDA: A new Pythonic Wind Retrieval Package, *Proc. of the 18th Python in Science Conference*, pp. 103-109
14. **X. Zheng**, **J.-C. Golaz**, **S. Xie**, Q. Tang, **W. Lin**, **M. Zhang**, H.-Y. Ma, **E. L. Roesler**: The summertime precipitation bias in E3SM Atmosphere Model Version 1 (EAMv1) over the Central United States, *Journal of Geophysical Research: Atmospheres*, https://doi.org/10.1029/2019JD030662, Accepted

9.1.2 Submitted and/or In Revision

1. **R. Jackson, S. Collis,** T. Lang, C. Potvin, and T. Munson, PyDDA: A Pythonic Direct Data Assimilation framework for wind retrievals, *J. Open Source Res. Software,* submitted, 2019

9.1.3 EOS Research highlights

- **Xie et al. (2019)**: Shultz, D. (2019), One step closer to a milestone in climate modeling, Eos, 100, https://doi.org/10.1029/2019EO129065. Published on 24 July 2019.

9.2 Regionally Refined Model (RRM) Configurations

- Five regionally refined configurations were supported and developed for the E3SM version 1 release. All RRM grid configurations have a low-resolution of 1-degree (~110km) and a high-resolution static patch of 1/4-degree (~25km). The high-resolution patches focus on Atmospheric Radiation Measurement (ARM) sites to further improve model development by housing a "ground-truth" based on ARM measurements and value-added products. These RRM meshes and their corresponding sites (in parentheses) include CONUS (SGP), North America (SGP and NSA), ENA (ENA), TWP (TWP), and the ARM West Antarctic Radiation Experiment.

9.3 Datasets

- 17 years of quality controlled corrected radar volumes and echo top heights from the CPOL Radar in Darwin. Currently available from ALCF/Petrel and in the process of being submitted to the ARM archive.
- 8 years of 3D winds derived from the CPOL Radar and ERA Interim over Darwin. We plan on submitting this as a PI product to the ARM archive.
- High-resolution 3D variational analysis of atmospheric states at 2km x 2km resolution from dynamically constrained WRF GSI and WRF simulations for the ARM MC3E May 20, 2011 convective event. Data are publicly available for download from http://cloud.somas.stonybrook.edu/mzhang/arm/MC3E/
- EAMv1 CAPT simulations with ENA RRM and ne30 during the ARM CAP-MBL field campaign (June 2009 to December 2010)
- EAMv1 CAPT simulations with CONUS RRM and ne30 for the time period from 1 June, 2011 to 31 August, 2011.

9.4 Software and tools

- **PyDDA** (Pythonic Direct Data Assimilation): A Pythonic Multiple Doppler Radar Wind Retrieval Package. Available at http://openradarscience.org/PyDDA. As a note of the software's impact for the community, it is going to be used by NASA for ground validation of GPM vertical vertical velocities in their Decadal Plan.
- **TINT** (TINT Is Not TITAN): A long-term cell tracking package that works directly with the Py-ART grid object in Python and is based on the Thunderstorm Identification, Tracking, Analysis and Nowcasting package (TITAN). Available as community code at https://github.com/openradar/TINT
- **StrideSearch**: a tool originally designed for identifying and tracking tropical and extratropical cyclones (e.g., climate and weather extremes) in global model output, this project supported further development of StrideSearch to search on unstructured grid meshes instead of exclusively latitudinal-longitudinal cartesian grids, search with a kd-tree algorithm, and search for mesoscale convective systems. https://github.com/pbosler/StrideSearch

- **Multi-Objective Optimization Framework package** for E3SM model tuning has been published on https://github.com/eexcalibur/GCM_paras_tune. A how-to document is included.

9.5 Student training

- Two Ph.D. students graduated (Haiyang Yu and Jingyi Chen) who were partially supported by the project; another two students, also partially supported by the project, are progressing toward completing their Ph.D. thesis (Jia Wang and Xiaoxi Zhu).
- Undergraduate student in computer science at the University of New Mexico, Matthew McChesney, was partially supported by this project to improve the process in developing a regionally refined model configuration and the Stride Search tool.
- Three SULI students were supported to work with cell tracking in Houston (Sam Carani, Jason Hemedinger and Brent Brock). Joel Porcarro, a SULI student, was partially supported to compare E3SM rainfall to Darwin diurnal cycle observed by the CPOL radar.

10 Appendix: references

Dai, A. (2006). Precipitation characteristics in eighteen coupled climate models. Journal of Climate, 19(18), 4605–4630, https://doi.org/10.1175/JCLI3884.1

Dai, A., & Trenberth, K. E. (2004). The diurnal cycle and its depiction in the Community Climate System Model. Journal of Climate, 17, 930–951. https://doi.org/10.1175/1520-0442(2004)017<0930:TDCAID>2.0.CO;2

Dixon, M., Wiener, G., 1993. TITAN: Thunderstorm Identification, Tracking, Analysis, and Nowcasting—A Radar-based Methodology. Journal of Atmospheric and Oceanic Technology 10, 785–797, https://doi.org/10.1175/1520-0426(1993)010<0785:TTITAA>2.0.CO;2

Fridlind, A.M., van Lier-Walqui, M., Collis, S., Giangrande, S.E., Jackson, R.C., Li, X., Matsui, T., Orville, R., Picel, M.H., Rosenfeld, D., Ryzhkov, A., Weitz, R., Zhang, P., 2019. Use of polarimetric radar measurements to constrain simulated convective cell evolution: a pilot study with Lagrangian tracking. Atmos. Meas. Tech. 12, 2979–3000, https://doi.org/10.5194/amt-12-2979-2019

Gray, W.M. and R.W. Jacobson, 1977: Diurnal Variation of Deep Cumulus Convection. Mon. Wea. Rev., 105, 1171–1188, https://doi.org/10.1175/1520-0493(1977)105<1171:DVODCC>2.0.CO;2

Helmus, J.J. & Collis, S.M., 2016: The Python ARM Radar Toolkit (Py-ART), a Library for Working with Weather Radar Data in the Python Programming Language. Journal of Open Research Software. 4(1), p.e25. DOI: http://doi.org/10.5334/jors.119

Jackson, R. C., Collis, S. M., Louf, V., Protat, A., and Majewski, L., 2018: A 17 year climatology of the macrophysical properties of convection in Darwin, Atmos. Chem. Phys., 18, 17687-17704, https://doi.org/10.5194/acp-18-17687-2018.

Louf, V., A. Protat, R.A. Warren, S.M. Collis, D.B. Wolff, S. Raunyiar, C. Jakob, and W.A. Petersen, 2019: An Integrated Approach to Weather Radar Calibration and Monitoring Using Ground Clutter and Satellite Comparisons. J. Atmos. Oceanic Technol., 36, 17–39, https://doi.org/10.1175/JTECH-D-18-0007.1

McKinney, W., 2010. Data Structures for Statistical Computing in Python, in: Walt, S. van der, Millman, J. (Eds.), Proceedings of the 9th Python in Science Conference. pp. 51–56.

Shultz, D. (2019), One step closer to a milestone in climate modeling, Eos, 100, https://doi.org/10.1029/2019EO129065

Thompson, E.J., S.A. Rutledge, B. Dolan, M. Thurai, and V. Chandrasekar, 2018: Dual-Polarization Radar Rainfall Estimation over Tropical Oceans. *J. Appl. Meteor. Climatol.,* 57, 755–775, https://doi.org/10.1175/JAMC-D-17-0160.1